ISSN: 2394-5311

Share Your Innovations through JACS Directory

Journal of Advanced Chemical Sciences

Visit Journal at https://www.jacsdirectory.com/jacs

Synthesis of Ag-Doped Lanthanum Nanoparticles using Simple Wet Chemical Process in Alkaline Medium; and Characterization of Optical, Morphological and Structural Properties

Hakim Q.N.M. Al-arique[1], Sameerah S.S. Alqadasy[2,*], Nabeel M.S. Kaawash[3], S.Q. Chishty[2], K.A. Bogle[3]

[1]*Department of Chemistry, Faculty of Applied Science, Taiz University, Taiz – 6803, Yemen.*
[2]*Department of Physics, Dr. Rafiq Zakaria College for Women, Dr. Babasahieb Ambedkar Marathwada University, Aurangabad – 341 004, Maharashtra, India.*
[3]*Thin Film and Device Laboratory, School of Physical Sciences, Swami Ramanand Teerth Marathwada University, Nanded – 431 606, Maharashtra, India.*

A R T I C L E D E T A I L S

Article history:
Received 22 August 2024
Accepted 14 September 2024
Available online 15 September 2024

Keywords:
Annealing Effect
Doping
Optical
Band Gap

A B S T R A C T

The manufacturing of doped semiconductor $Ag_2O.La_2O_3$ (Ag-La) nanoparticles (NPs) in an alkaline medium at 60–70 °C is described in this paper, utilising a straightforward wet chemical procedure. Numerous tools are used to characterise Ag-La NPs, such as ultraviolet/visible spectroscopy (UV/Vis.), field emission scanning electron microscopy (FE-SEM), Fourier transform infrared spectroscopy (FTIR), and powder X-ray diffractometer (XRD). An X-ray diffraction analysis revealed that the Ag-doped Nps are polycrystalline in nature and crystallise in a hexagonal phase with crystallites oriented in various directions. The morphology of the particles shows layers of aggregation of different sized and shaped nanosheets. Studies on their optical properties, however, have revealed that absorption takes place in the 270–291 nm range and that the transmission value, which ranges from 30 to 64%, is influenced by the temperature during annealing. An increase in annealing temperature results in a corresponding drop in band gap energy, from 4.27 to 4.10 eV.

1. Introduction

Nano structuring have been a promising strategy due to realize factorial of their prestigious physiochemical properties such as thermal stability, optical property, crystal structure, electrical conductivity, magnetic properties, mechanical strength, catalytic activity, and these materials receive greater research attention due to their application probability in different zones of technology [1,2]. Nanocomposites have become more commercially used due to their multiple technological uses in the production of multiple technological applications and an extensive variety of consumer products in the field of biological, food industry, pharmaceutical industries, chemical industries, sensing, energy conversion and storage devices etc., [3,4]. The increased development of the nanomaterial properties paved the way for researchers to produce innovative and novel materials in the future for the improvement possibility of the quality of life. In the same way, advance research on nanomaterials are showed that doped metal oxide nanomaterial by doping or co–doping with transition or semiconductor metal ions in different proportions into pure intrinsic semiconductor due to their excellent and enhanced physiochemical properties [5,6].

Additionally, doped semiconductor nanostructure materials can be employed in newly designed electrodes as electron mediators in order to apply electrochemical sensing devices to detect different toxic substances in our ecosystem [7]. As a result, numerous research using various electrochemical techniques to probe different toxic compounds as well as biomolecules have been described, involving the use of doped or un-doped nanomaterials [8,9]. Due to their varying valence states, rare earth (RE) metal oxides have promising optical, magnetic, and electrical conductivity properties [10,11]. Lanthanum oxide (La_2O_3) has aroused great research interests due to its remarkable electrical, thermal, optical, stability, non–toxicity, biocompatibility and chemical properties [4]. Application of lanthanum oxide nanoparticles with antibacterial properties was developed by Muthu Lakshmi et al. using extract from leaves of *Andrographis paniculata* [2]. Electrochemical vapor deposition was used by No et al. to produce lanthanum oxide thin films, and their electrical characteristics were examined [12]. Nieminen et al. prepared a lanthanum oxide thin film, which they then examined for chemical stability in the surrounding air [13]. A lot of interest has been shown recently in Rare earth (RE) metal oxide, which varies in composition, texture, and 4f electron presence [14].

Additionally, La_2O_3 thin films are getting more attentions due to their numerous uses in glass ceramic, gas sensors, and super capacitors. Depending on the methods of film deposition and heat treatment, La_2O_3 thin films can exist in a variety of crystalline phases, including cubic (c–La_2O_3), hexagonal (h–La_2O_3), amorphous (a–La_2O_3), and a combination of the phases [15].

Different techniques, including electrospinning, electrodeposition, and acoustically controlled microbubble formation, have been used to generate porous materials, which have improved their super capacitive, catalytic, and sensing capabilities, and as a result of two different species coexisting, mixed transition metal oxides have demonstrated the potential to enhance specific capacitance by diversifying redox processes [16,17]. Usually, Ag nanostructures are typically superior to other precious metals in terms of their physical and chemical properties [18]. As a result, they have been extensively researched and used in a variety of applications, including optical sensors, biological diagnostics, catalysis, microelectronics, etc.,. Also, Ag has demonstrated excellent antibacterial and antifungal activities due to its high cytotoxicity against a wide variety of microorganisms [19]. The unique qualities of lanthanum and silver nanoparticles—including their optical, magnetic, thermal, catalytic, sensing, electrochemical, antibacterial, and antioxidant capabilities have drawn a great deal of interest and in addition to the magnetic as well as multilevel storage property as an application in electrochemical metallization memory (ECM) devices [20]. According to this paradigm, we believe a promising method for detecting toxic compounds is the Ag doping in La materials. As of right now, the silver composite lanthanum substance has not been the subject of any such reports. As a result, in this work, lanthanum and silver were combined to synthesized doped semiconductor nanostructure metal oxides $Ag_2O–La_2O_3$ with improved electrical performance through wet chemical methods [21].

Herein the synthesized doped semiconductor nanomaterial $Ag_2O–La_2O_3$ was highly sensitive to thiourea (CH_4N_2S) based on sensor by using reliable electrochemical technique. $SC–(NH_2)_2$ is the molecular formula for thiourea, commonly referred to as thiocarbamide, which is an organosulfur chemical. Owing to its toxic qualities, it contributes to pollution, which damage the ecosystem's sustainability. Even though thiourea is toxic, its derivatives work well for the administration of medications. It has been demonstrated through research that thiourea

*Corresponding Author:sameerahalqadasy@gmail.com(Sameerah S.S. Alqadasy)

https://doi.org/10.30799/jacs.260.24100302

Cite this Article as: Hakim Q.N.M. Al-arique, Sameerah S.S. Alqadasy, Nabeel M.S. Kaawash, S.Q. Chishty, K.A. Bogle, Synthesis of Ag-doped lanthanum nanoparticles using simple wet chemical process in alkaline medium; and characterization of optical, morphological and structural properties, J. Adv. Chem. Sci. 10(3) (2024) 803–807.

derivatives have antibacterial, antioxidant, and HIV therapeutic applications. Nanomaterials have therefore been used as sensors for the adsorption of well-known toxic gases and drug delivery [22,23]. Therefore, in this study, we report the successful use of the simple versatile, economical and cost effective wet chemical procedure to synthesis of Ag–La NPs and study the effect of annealing temperature on the structural, optical, and morphological characteristics of the prepared NPs.

2. Experimental Methods

2.1 Materials and Methods

All of the analytical-grade chemicals utilised in this experiment were bought from the Indian branch of Sigma-Aldrich Chemise. The manufacture of doped $Ag_2O.La_2O_3$ NPs was accomplished using a simple wet chemical procedure. In this procedure, 250 mL of an Erlenmeyer flask were filled with equimolar (0.1 M) solutions of reactive species $LaCl_3.7H_2O$ (99.99%) and $AgNO_3$ (99.9%), and was to homogenise the mixture frequent stirring was used. As a stabilising agent for the de-agglomeration of precursors and product (nanoparticles), 100 mL of the thiourea (CH_4N_2S) same concentration was added to the same flask as well, and the flask was well shaken following the addition of thiourea. (2.0 M) solution of NaOH was added slowly so as to shift the pH of the medium at alkaline side and adjusted at 10. After that, the reaction flask was heated at 60-70 °C for 4 hours with continuous stirring on electric hot plate in order to get the precipitates of Ag-La at the end point it was formed as a co-precipitation and then it was filtered and washed with the plenty of distilled water plus acetone to remove the undesired impurities if present. Afterward it was dried at 100 °C in an oven for 10 hours. It was ground to create homogeneity after drying. The powder is then split into four portions. The first part is un-annealed, and the subsequent sections are annealed at various temperatures (500, 700, and 900 °C). After that, the sample is put through testing.

2.2 Characterization

In order to evaluate the crystallite phase and phase purity of the particles Rigaku Ultima III (CuKα, 40 kV, 40 mA, 1.54 Å) x-ray diffraction (XRD) unit was used with scan step of 0.02° (θ) in scanning range between 10° and 80°. The morphology of Ag-La nanoparticles was investigated by (SEM) FESEM–JEOL JEM–6360 Mira–3, Tascan, Republic of Czech. for the substance's purity verification, Fourier transform infrared (FT-IR JASCO-4600) spectra were analysed from 400 to 4000 cm^{-1}, the transmittance mode was used for this examination at room temperature. Optical characterizations were performed in the wavelength range of 300–900 nm by Ultraviolet–visible spectrophotometer (Perkin Elmer 45 UV–VIS).

3. Results and Discussion

3.1 Structural Properties: X-Ray Diffraction (XRD) Analysis

The XRD patterns of Ag- La NPs, both un-annealed and annealed at different temperatures (500, 700, and 900 °C), are shown in Fig. 1. Using powdered XRD analysis, we looked at the crystallinity of our synthesised Nps in the (2θ) range of 10–80°, all of the diffraction peaks in the pattern may be indexed as the hexagonal phase. Additionally, even though the XRD patterns show peak widening prior to annealing due to the tiny size of the crystallites, the crisp diffraction peaks show excellent crystallisation of Ag-La NPs. It was observed that every sample generated had a polycrystalline structure. The principal peaks are at 2θ = 28.8°, 38°, and 44.3°, with some weak peaks appearing, dependent on annealing, temperature. and many peaks for un-annealed sample that fade after annealing process.

The data obtained from the experiment indicate the existence of several distinct peaks at certain angles at 2θ= 28.8° (100), 30° (101) corresponding to $AgO_2.La_2O_3$ NPs [24-27]. 33° (111), 38° (011), 44.3° (200), 45° (211), 64° (204), 77.4° (311) corresponding to AgO_2 [6, 28,29] and 15.8° (101) [30,31]. 23.7° (021), 24.2° (021), 26° (100), 39.5° (102) are related to La_2O_3 [6, 24, 25].

It is significant to observe that the NPs' crystallinity has improved after annealing at various temperatures Fig. 1. In addition, a fresh rearrangement of the crystal lattice causes the XRD to move to a low angle and produce new peaks [32]. There are many peaks in case of un-annealed particles, but after annealing, many peaks disappeared, and some shifted the location. The existence of several diffraction peaks with different strengths suggests that Ag-La is growing on different crystallographic planes, which is indicative of anisotropic growth. Peak intensity is shown to increase and full width at half maximum (FWHM) values to decrease with increasing annealing temperature. These patterns imply the existence of bigger crystallite sizes, which would enhance the quality of the crystals of the synthetic NPs [33–35]. The study found that when temperature rose, crystallite size increased, dislocation density, and strain decreased, as shown in Fig. 2(a and b) and Table 1. Grain boundaries are reduced as a result of the expansion of the crystal phase, which is caused by the enlargement of crystals through the fusion of microcrystals. The annealing process is responsible for the observed phenomena of greater crystallinity and increased crystallite size. This is because there is enough energy available for atomic diffusion towards more ordered places. Generally speaking, one of the best ways to reduce internal stresses in NPs materials is to apply heat treatment after deposition [36,37]. The crystallite grain size (D) in the film microstructure was calculated using the Scherrer formula [38],

$$D = \frac{K\lambda}{\beta Cos\theta} \quad (1)$$

where k is a constant taken to be 0.94, λ is the X-ray wavelength (λ = 0.1540598 nm), and β is the full width at half maximum value (FWHM) of the peak in radians. The relationship between dislocation density and lattice strain, particularly at the micro level, is widely acknowledged to exhibit a reduction as the size of crystallites rises, the reduced occurrence of grain boundaries in the NPs to the decrease in lattice defects as the size of the crystallite grows at higher temperatures [39].

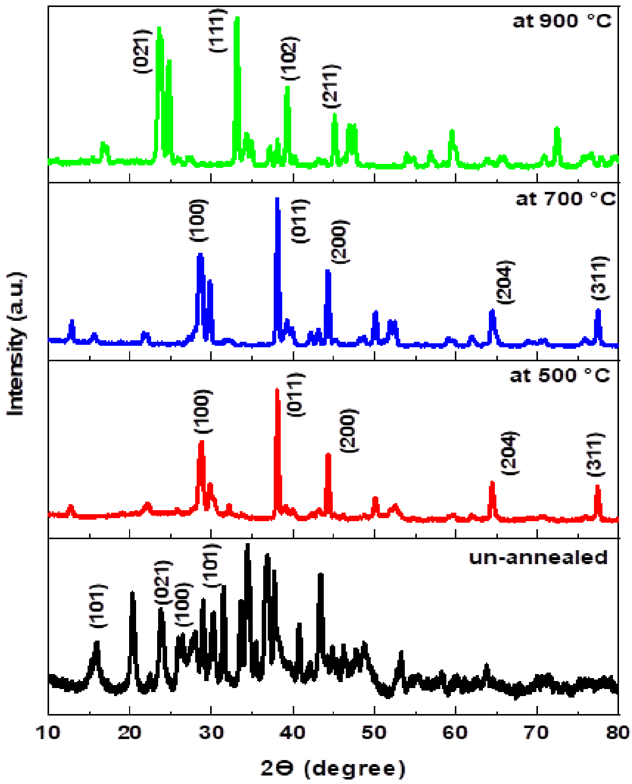

Fig. 1 X-ray diffraction patterns of Ag-La NPs un-annealing and after annealing at various temperatures (500, 700, 900 °C)

The length of dislocation lines per unit volume is defined by the dislocation density (δ). It represents the number of defects in the NPs and is estimated as [40]:

$$\delta = \frac{1}{D^2} \quad (2)$$

The strain (ε) in the NPs microstructure is evaluated as [40]:

$$\varepsilon = \frac{\beta}{4\, tan\theta} \quad (3)$$

and interlayer distance calculated from the Bragg's law [41]:

$$d = \frac{n\lambda}{2Sin\theta} \quad (4)$$

Table 1 Variation of crystallites size, dislocation density δ, and lattice strain of Ag-La NPs un-annealing and after annealing at various temperatures (500, 700, 900 °C)

Parameters	Un-annealed	at 500 °C	at 700 °C	at 900 °C
D (nm)	19.06	19.26	20.3	20.88
d (nm)	0.248	0.283	0.262	0.229
$\delta \times 10^{-3}$ (nm^{-2})	3.57	4.68	3.05	3.01
$\varepsilon \times 10^{-3}$	9.16	8.43	7.2	6.8

https://doi.org/10.30799/jacs.260.24100302

Cite this Article as: Hakim Q.N.M. Al-arique, Sameerah S.S. Alqadasy, Nabeel M.S. Kaawash, S.Q. Chishty, K.A. Bogle, Synthesis of Ag-doped lanthanum nanoparticles using simple wet chemical process in alkaline medium; and characterization of optical, morphological and structural properties, J. Adv. Chem. Sci. 10(3) (2024) 803–807.

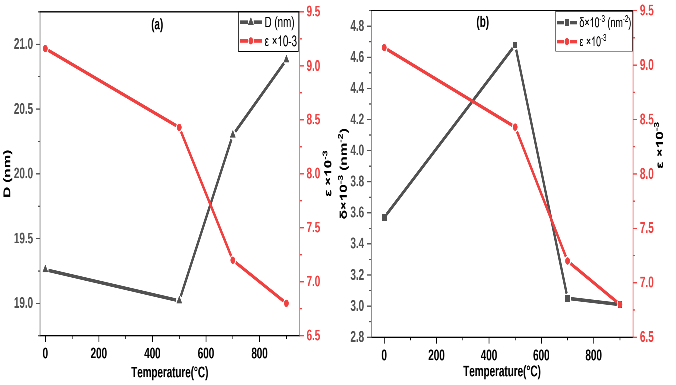

Fig. 2 a) Variation of (ε) and (D), **b)** Variation of (δ) and (ε) with temperature of Ag-La NPs un-annealing and after annealing at various temperatures (500, 700, 900 °C)

3.2 Fourier Transform Infrared (FTIR) Spectra

FTIR studies are crucial to establish the development of the samples nanocrystals and to detect any substances that have been adsorbed onto the film's surface. FTIR spectrum products for un-annealed and after-annealed NPs were performed to understand these materials' structure and composition better. Fig. 3 displays the Fourier transform infrared (FTIR) spectra at room temperature in the range of 400–4000 cm^{-1} of Ag-La NPs before and after annealing at different temperatures. Significantly, the recorded data exhibited prominent peaks falling within the spectral region of 1330–1520 cm^{-1}, indicating the likely existence of C-H, peak at 850 cm^{-1} that of stretching bond of C-Cl [42], a weak peak at 650 cm^{-1} that belongs to Ag-O [43] and a peak at 470 [44,32], 416 cm^{-1} [45] that belongs to La-O in case of un-annealed sample [27,32, 44]. But after annealing, new peaks appear at wave numbers 594 cm^{-1} [27]. 1098, 1058 cm^{-1} [44] and 1179 cm^{-1} are corresponding to La-O, C=O [46,32], and S=O respectively [42].

Annealing at different temperatures has been seen to result in a solution suitable for guaranteeing the effective integration of Ag and La atoms. The position and strength of the peak vary as a result of doping and annealing. This clearly shows that there is a difference in the binding strength of the doping substance. Due to their superior adsorption capabilities and attractive uniformity, these Nps hold tremendous promise for constructing innovative, which employed for many industrial and environmental applications [47].

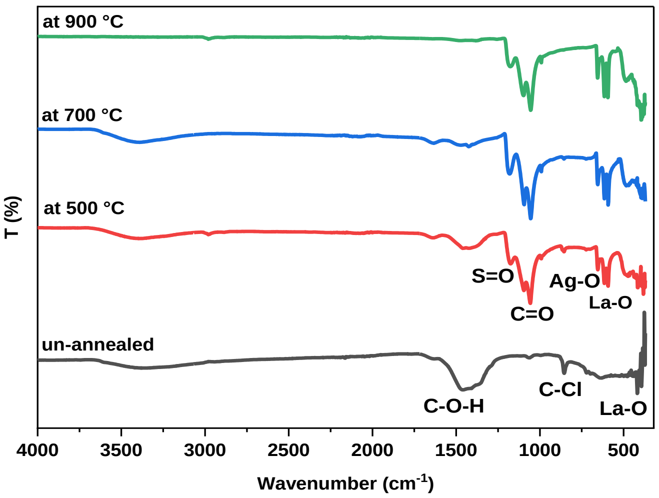

Fig. 3 FTIR spectrum of Ag-La NPs un-annealing and after annealing at various temperatures (500, 700, 900 °C)

3.3 Morphological Properties: Field Emission Scanning Electron Microscopy (FE-SEM)

The particle morphology before and after annealing at various temperatures is as shown in Fig. 4. The Ag-La particles had a considerable propensity to aggregate; the morphology of the samples varies with temperature, as was noticed. Fig. 4(a) shows there are a variety of morphologies, with distinct agglomerations and varied shapes and sizes for the un-annealing sample [48]. Particles consist of aggregates with flat shapes and almost no visible crystalline surfaces. Particles with rough, complex surfaces are seen in high magnification micrographs (Fig. 4(b)). This data suggests that the created particles may have originated from the annealing aggregation of smaller individuals (of nonmetric dimensions) at 500 °C [49].

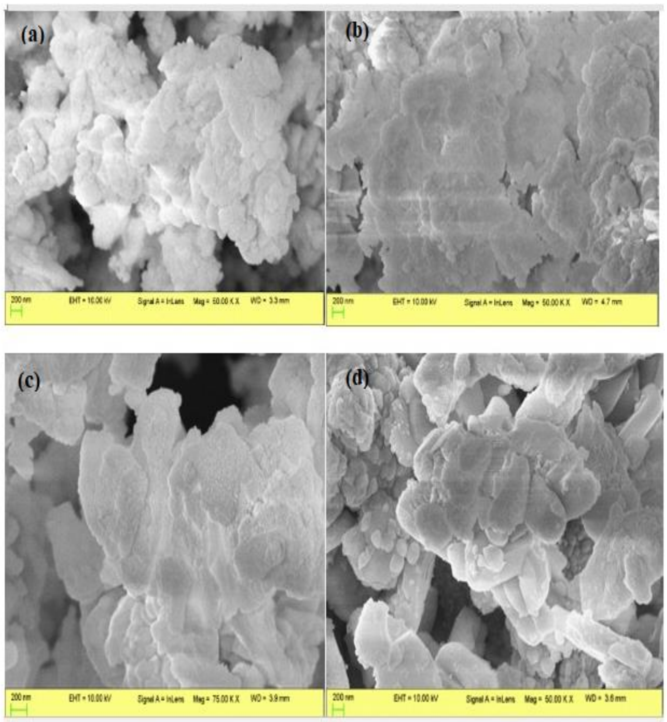

Fig. 4 FE-SEM of Ag-La NPs, (a) un-annealing and after annealing at various temperatures (b) 500 °C, (c) 700 °C, and (d) 900 °C

The particles are made up of tiny, irregularly formed particles that are only a few micrometres in size [50,51]. An increase in particle size results in a smoother surface when the annealing temperature rises to 700 °C. According to electron micrographs, the constituent particles seem larger in size, and the strength of the particle aggregates weakens, forming compact nanosheets at the greatest annealing temperature 900 °C [52].

The rise in temperature resulted in an observed increase in the average grain sizes of the Ag-La NPs this can be attributed to the enhanced mobility of surface atoms and increased cluster formation. Consequently, the coalescence of smaller grains was expedited during the thermal processing stage [53-54].

3.4 UV–Vis Spectroscopy: Optical Properties

The absorbance curve from the UV-VIS spectrophotometer as a function of wavelengths is displayed in Fig. 5(a). The NPs all exhibited high absorption in the ultraviolet region, with absorption edges in the electromagnetic spectrum's range of 270–291 nm with the highest intensity of 1.30 for un-annealed sample. After annealing, the absorption edge decrees, reaching a minimum value of absorption at 700 °C (0.28) before rising again at 900 °C to 0.400, while the Nps' absorption in the visible region increased as wavelength increased. Annealing causes materials to crystallize; the electrical structure of the material can change as it gets more crystalline, which changes the band structure and its absorption characteristics, which shifts the absorption edge. The optical transmittance spectra of Ag-La Nps are shown in Fig. 5(b). According to the findings, Ag-La Nps exhibit strong transmittance in the UV spectrum between 200 and 300 nm and increase with annealing temperatures, Table 2.

Table 2 The variation of absorption, transmission, and bandgap energy of Ag-La NPs un-annealing and after annealing at various temperatures (500, 700, 900 °C)

Parameters	Un-annealed	500 °C	700 °C	900 °C
Absorption (nm)	270	291	285	291
Transmission (%)	30-27	39-30	64-51	50-32
E_g(eV)	4.63	3.66	4.22	4.17

Conversely, following annealing, transmittance curves gradually indicate drops in the visible area. Because of certain existing imperfections in the particles which are mostly caused by the Ag-La NPs surface roughness the transmittance value comparatively drops [55]. Larger crystal sizes produced by higher annealing temperatures have an impact on the specific surface area of the nanomaterial, which in turn affects light scattering. Still, there is a significant influence of phase composition and crystal diameters on the bandgap. Lower bandgap energies (E_g) have been caused by structural modifications and decreased interatomic separation as the annealing temperature has increased, Table 2.

https://doi.org/10.30799/jacs.260.24100302

Cite this Article as: Hakim Q.N.M. Al-arique, Sameerah S.S. Alqadasy, Nabeel M.S. Kaawash, S.Q. Chishty, K.A. Bogle, Synthesis of Ag-doped lanthanum nanoparticles using simple wet chemical process in alkaline medium; and characterization of optical, morphological and structural properties, J. Adv. Chem. Sci. 10(3) (2024) 803–807.

The bandgap energy is significantly influenced by the thermal stresses and the quantum size impact encountered in the annealing. The increase in grain size seen in SEM pictures and XRD results is confirmed by the lower bandgap energies at higher annealing temperatures [56].

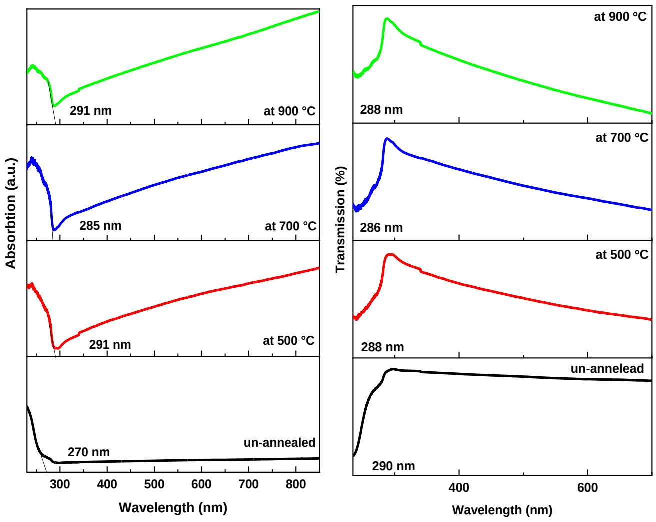

Fig. 5 a) Absorption spectra, **b)** transmittance spectrum of Ag-La NPs un-annealing and after annealing at various temperatures (500, 700, 900 °C)

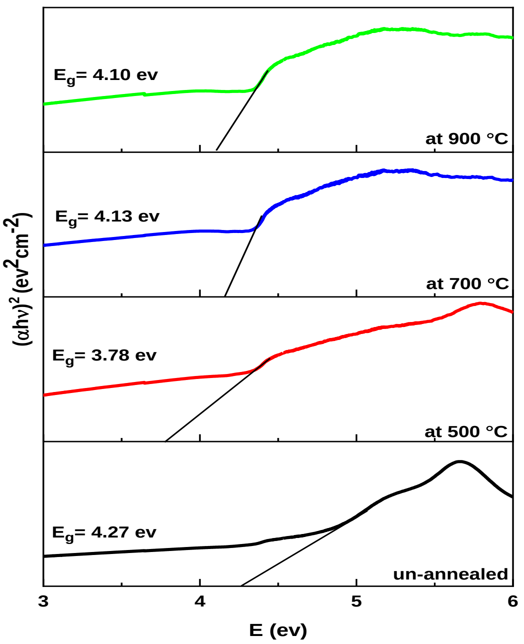

Fig. 6 The optical band gap E_g of Ag-La NPs un-annealing and after annealing at various temperatures (500, 700, 900 °C)

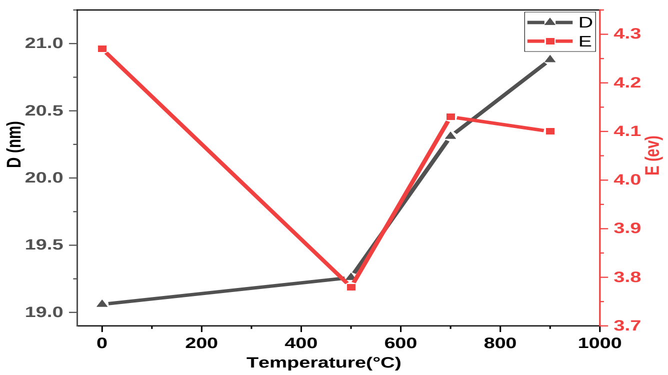

Fig. 7 Variation of (E_g) and (D) of Ag-La NPs with annealing temperature

The Tauc model is used to compute the energy band gap (E_g) of NPs [57].

$$(\alpha h\nu)^2 = A\left(h\nu - E_g\right) \quad (5)$$

where α is the absorption coefficient, hv is the photon energy, A is a constant, and E_g is the optical bandgap. The quantum size effect is responsible for the observed rise in E_g from 3.78 to 4.10 eV when the annealing temperature rises from 500 to 900 °C, indicating that E_g is highly sensitive to the annealing temperature [58]. The findings are displayed in Fig. 6 and Table 2.

The observed phenomenon of the valence band shifting upwards and the conduction band shifting downwards can be explained by the enlarged defect levels at these specific sites, leading to the narrowing of the band gap. Furthermore, it has been discovered that there is a reduction in the E_g value as the grain size are grows Fig. 7. The observed behaviour can be ascribed to fluctuations in crystallinity, distribution of dopants, the quantum size effect, and stresses present within the films [59-61].

4. Conclusion

The synthesis of lanthanum oxide doped with Ag is synthesised and XRD, FESEM, FTIR, and UV/Vis were used to characterise the structural, morphological, and optical properties of $Ag_2O.La_2O_3$ NPs. Every sample's generated Nps crystallites, according to X-ray diffraction examination, are polycrystalline in nature and crystallise in a hexagonal phase with crystallites oriented in different directions. The results of the FTIR spectroscopy research demonstrate the variation of Ag-La Nps that were both un-annealed and annealed in air for two hours at various temperatures. Conversely, changes in annealing temperatures result in variations in the values of the band gap energy, transmission, and absorption. The fact that these results were produced with a common, affordable, alkaline wet chemical method makes them quite fascinating technique which has been used to produce this kind of doped oxide establishing the path for the possible commercialization of Nps in a range of applications, including sensing and photocatalysis.

References

[1] I. Sosa, C. Noguez, R. Barrera, Optical properties of metal nanoparticles with arbitrary shapes. J. Phys. Chem. B 107 (2003) 6269–6275.

[2] V. Muthulakshmi, M. Balaji, M. Sundrarajan, Ionic liquid mediated morphologically improved lanthanum oxide nanoparticles by *Andographis paniculata* leaves extract and its biomedical applications, J. Rare Earths 38 (2020) 281–291.

[3] W. Lee, K. Kim, N. Gurudatt, K. Hussain, C. Choi, D. Park, Y. Shim, Comparison of enzymatic and non-enzymatic glucose sensors based on hierarchical Au-Ni alloy with conductive polymer, Biosens. Bioelectron. 130 (2019) 48–54.

[4] S. Jadhav, D. Malavekar, R. Bulakhe, U. Patil, I. Insik, C. Lokhande, P. Pawaskar. Dual-Functional electrodeposited vertically grown $Ag-La_2O_3$ nanoflakes for non-enzymatic glucose sensing and energy storage application, Surf. Interf. 23 (2021) 101018.

[5] I. Hussain, N. Singh, A. Singh, H. Singh, S. Singh, Green synthesis of nanoparticles and its potential application, Biotechnol. Lett. 38 (2016) 545–560.

[6] M. Rahman, T. Sheikh, A. Asiri, M. Awual, Development of 3-methoxyanaline sensor probe based on thin $Ag_2O@La_2O_3$nanosheets for environmental safety, New J. Chem. 43 (2019) 4620-4632.

[7] X. He, W. Aker, P. Fu, H. Hwang, Toxicity of engineered metal oxide nanomaterials mediated by nano-bio-eco-interactions: A review and perspective, Environ. Sci. Nano 2 (2015) 564–582.

[8] J. Kulys, V. Simkeviciene, I. Higgins, Concerning the toxicity of two compounds used as mediators in biosensor devices: 7, 7, 8, 8-tetracyanoquinodimethane (TCNQ) and tetrathiafulvalene (TTF), Biosens. Bioelectron. 7 (1992) 495-501.

[9] M. Rahman, M. Alam, A. Asiri, Sensitive 1,2 dicjolorobenzenechemi-sensor development based on solovthermally prepared FeO/CdO nanocubes for environmental safety. J. Ind. Eng. Chem. 62 (2018) 392–400.

[10] T. Sasaki, Y. Matsumoto, J. Hombo, Y. Ogawa, A new preparation method of $LaMnO_3$ perovskite using electrochemical oxidation, J. Sol. State Chem. 91 (1991) 61-70.

[11] B. Jaffar, H. Swart, H. Ahmed, A. Yousif, R. Kroon, Stability of Bi doped La_2O_3 powder phosphor and PMMA composites, J. Phys. Chem. Solids 131 (2019) 156-163.

[12] S. No, D. Eom, C. Hwang, H. Kim, Properties of lanthanum oxide thin films deposited by cyclic chemical vapor deposition using tris (isopropyl-cyclopentadienyl) lanthanum precursor, J. Appl. Phys. 100 (2006) 024111.

[13] M. Nieminen, M. Putkonen, L. Niinistö, Formation and stability of lanthanum oxide thin films deposited from β-diketonate precursor, Appl. Surf. Sci. 174 (2001) 155-166.

[14] V. Mane, D. Malavekar, S. Ubale, R. Bulakhe, I. Insik, C. Lokhande, Binder free lanthanum doped manganese oxide @ graphene oxide composite as high energy density electrode material for flexible symmetric solid state super capacitor, Electrochim. Acta 335 (2020) 135613.

[15] C. Ramana, S. Vemuri, V. Kaichev, A. Kochubey, A. Saraev, V. Atuchin, X–ray Photoelectron spectroscopy depth profiling of La_2O_3/Si thin films deposited by reactive magnetron sputtering, ACS Appl. Mater. Interf. 3 (2011) 4370–4373.

[16] S. Jin, X. Wei, Z. Yu, J. Ren, Z. Meng, Z. Jiang, Acoustic-controlled bubble generation and fabrication of 3D polymer porous materials, ACS Appl. Mater. Interf. 12 (2020) 22318–22326.

[17] S. Park, H. Boo, T. Chung, Electrochemical non-enzymatic glucose sensors, Anal. Chim. Acta 556 (2006) 46–57.

https://doi.org/10.30799/jacs.260.24100302

Cite this Article as: Hakim Q.N.M. Al-arique, Sameerah S.S. Alqadasy, Nabeel M.S. Kaawash, S.Q. Chishty, K.A. Bogle, Synthesis of Ag-doped lanthanum nanoparticles using simple wet chemical process in alkaline medium; and characterization of optical, morphological and structural properties, J. Adv. Chem. Sci. 10(3) (2024) 803–807.

[18] S. Yang, K. Wu, Y. Zhang, H. Liu, P. Li, C. Wu, K. Yan, 2D Ag ion-loaded anionic nanosheets for polymer-based film with durable antibacterial activities, ACS Omega 7 (2022) 33858–33865.

[19] A. Wang, M. Shao, F. Yang, F. Chen, Preparation and properties of antibacterial PVDF composite thin films, Eur. Polym. J. 160 (2021) 110803.

[20] K. Wang, Y. Wu, H. Li, M. Li, F. Guan, H. Fan, A hybrid antioxidizing and antibacterial material based on Ag–La_2O_3 nanocomposites, J. Inorg. Biochem. 141 (2014) 36–42.

[21] M. Rahman, A. Asiri, 3-Methoxyphenol chemical sensor fabrication with Ag_2O/CB nanocompositions. New J. Chem., 42 (2018) 3936–3946.

[22] H. Saleem, S. Zaidi, Recent Developments in the Application of Nanomaterials in Agroecosystems, Nanomater. 10 (2020) 2411-2445.

[23] L. Mtescu, M. Chifiriuc, C. Postolache, G. Pircalabioru, A. Bolocan, Nanoparticles' toxicity for humans and environment, in: Nanomaterials for Drug Delivery and Therapy, William Andrew Publishing, Elsevier, Norwich, New York, 2019, pp.515–535.

[24] H. Kabir, S. Nandyalaa, M. Rahman, M. Kabir, Z. Pikramenou, M. Laver, A. Stamboulis, Polyethylene glycolassisted facile sol-gel synthesis of lanthanum oxide nanoparticles: Structural characterizations and photoluminescence studies, Ceram. Int. 45 (2018) 424-431.

[25] W. Gu, Y. Song, J. Liu, F. Wang, Lanthanum-based compounds: Electronic bandgap-dependent electro-catalytic materials toward oxygen reduction reaction, Chemistry - Europ. J. 23 (2017)10126-10132.

[26] A. Yadava, A. Lokhandeb, J. Kim, C. Lokhande, Highly sensitive CO_2 sensor based on microrods-like La_2O_3 thin film electrode, RSC Adv. 6 (2016) 106074-106080.

[27] W. Khalaf, M. Al-Mashhadani, Synthesis and characterization of lanthanum oxide La_2O_3 Net-like Nanoparticles by New Combustion Method, Biointerface Res. Appl. Chem. 12 (2022) 3066–3075.

[28] E. Salim, M. Awayiz, R. Mahdi, Tea concentration effect on the optical, structural, and surface roughness of Ag_2O thin films, Dig. J. Nanomater. Biostruct. 14 (2019) 1151-1159.

[29] K. Jyoti, M. Baunthiyal, A. Singh, Characterization of silver nanoparticles synthesized using *Urticadioica* Linn. leaves and their synergistic effects with antibiotics, J. Radiat. Res. Appl. Sci. 9 (2016) 217-227.

[30] K. Mustofa, Y. Yulizar, A. Saefumillah, D. Apriandanu, La_2O_3 nanoparticles formation using *Nothopanax scutellarium* leaf extract in two-phase system and photocatalytic activity under UV light irradiation, Mater. Sci. Eng. 902 (2020) 012018.

[31] R. Jbeli, A. Boukhachem, F. Saadallah, S. Alleg, M. Amlouk, H. Ezzaouï, Synthesis and physical properties of Fe doped La_2O_3 thin films grown by spray pyrolysis for photocatalytic applications, Mater. Res. Express 6 (2019) 066414.

[32] R. Jbeli, A. Boukhachem, I. Jemaa, N. Mahdhi, F. Saadallah, H. Elhouichet, S. Alleg, M. Amlouk, H. Ezzaouïa, An enhancement of photoluminescence property of Ag doped La_2O_3 thin films at room temperature, Spectrochim. Acta A. 184 (2017) 71-81.

[33] P. Singh, A. Kumar, D. Kaur, ZnO nanocrystalline powder synthesized by ultrasonic mist-chemical vapour deposition, Opt. Mater. (Amst). 30 (2008) 1316–1322.

[34] H. Belkhalfa, H. Ayed, A. Hafdallah, M. Aida, R. Ighil, Characterization and studying of ZnO thin films deposited by spray pyrolysis: Effect of annealing temperature, Optik (Stuttg). 127 (2016) 2336–2340.

[35] A. Saleh, A. Mohammad, Z. Khodair, N. Bakr, The influence of annealing temperature on structural and optical properties of ZnO nanostructures thin films grown using hydrothermal technique, The 1st Iran-Kurdistan International Conference on Physics, Iran, 2021.

[36] J. Park, Y. Hong, S. Kim, Growth of ZnO thin films by metalorganic chemical vapor deposition using isopropyl alcohol for oxygen precursor, Mater. Sci. Forum 510–511 (2006) 998–1001.

[37] H. Lee, J. Lee, T. Kim, D. Kim, W. Cho, Formation mechanism of preferential c-axis oriented ZnO thin films grown on p-Si substrates, J. Mater. Sci. 39 (2004) 3525–3528.

[38] X. Cheng, H. Zhao, L. Huo, S. Gao, J. Zhao, ZnO nanoparticulate thin film: Preparation, characterization and gas-sensing property, Sens. Actuators B Chem. 102 (2004) 248–252.

[39] I. Sutapa, A. Wahab, P. Taba, N. Nafie, Dislocation, crystallite size distribution and lattice strain of magnesium oxide nanoparticles, J. Phys. Conf. Ser. 979 (2018) 012021.

[40] H. Cai, K. Tuokedaerhan, Z. Lu, R. Zhang, H. Du, Effect of annealing temperature on the structural, optical, and electrical properties of Al-Doped ZrO_2 gate dielectric films treated by the sol–gel method, Coatings 12 (2022) 1837.

[41] N. Kaawash, D. Narwade, P. Alegaonkar, K. Bogle, Rationally desined state-of-the art approach for enhancing the ultraviolet photon detection performance of ZnO thin film, Phys. B Condens. Matter. 648 (2023) 414396.

[42] C. Yuen, S. Ku, P. Choi, C. Kan, S. Tsang, Determining functional groups of commercially available ink-jet printing reactive dyes using infrared spectroscopy, Res. J. Text. Apparel. 9 (2005) 26-39.

[43] Grey I. Waterhouse, G. Bowmaker, J. Metson, The thermal decomposition of silver (I, III) oxide: A combined XRD, FT-IR and Raman spectroscopic study, Phy. Chem. Chem. Phy. 3 (2001) 3838-3845.

[44] A. Umar, A. Ibrahim, R. Kumar, T. Almas, P. Sandal, M. Al-Assiri, M. Mahnashi, B. AlFarhan, S. Baskoutas, Fern shaped La_2O_3 nanostructures as potential scaffold for efficient hydroquinone chemical sensing application, Ceram. Int. 46 (2020) 5141-5148.

[45] L. Radev, L. Pavlova, B. Samuneva, E. Kashchieva, I. Mihailova, M. Zaharescu, B. Malic, L. Predoana, Sol-gel synthesis and structure of La_2O_3–CoO–SiO_2 powders, Process. Appl. Ceram. 2 (2008) 103–108.

[46] S. Arulkumar, M. Sabesan, Rapid preparation process of antiparkinsonian drug Mucunapruriens silver nanoparticle by bioreduction and their characterization, Pharmacog. Res. 2 (2010) 233-236.

[47] L.E. Brus, A simple model for the ionization potential, electron affinity, and aqueous redox potentials of small semiconductor crystallites, J. Chem. Phys. 79 (1983) 5566–5571.

[48] A. Fahrina, N. Arahman, S. Mulyati, S. Aprilia, N. Nawi, A. Aqsha, M. Bilad, R. Takagi, H. Matsuyama, Development of Polyvinylidene fluoride membrane by incorporating bio-based ginger extract as additive, Polymers 12 (2020) 2003-2014.

[49] A. Giaccherini, A. Griesi, G. Montegrossi, M. Romanelli, G. Lepore, A. Lavacchi, G. Amthauer, G. Redhammer, G. Tippelt, S. Martinuzzi, G. Cucinotta, M. Mannini, A. Caneschi, F. Benedetto, A new solvothermal approach to obtain nanoparticles in the Cu_3SnS_4–Cu_2FeSnS_4 join, J. Geosci. 65 (2020) 3–14.

[50] Z. Kayani, S. Riaz, S. Naseem, Structural and magnetic properties of the thin film of cobalt nitride, Surf. Rev. Lett. 21 (2014) 1450081.

[51] E. Falletta, C. Bianchi, F. Morazzoni, A. Polissi, F. Vincenzo, I. Bellobono, Tungsten trioxide and its TiO_2 mixed composites for the photocatalytic degradation of NOx and bacteria (*Escherichia coli*) inactivation, Catalysts 12 (2022) 822-838.

[52] T. Foley, C. Johnson, K. Higa, Inhibition of oxide formation on aluminum nanoparticles by transition metal coating, Chem. Mater. 17 (2005) 4086-4091.

[53] Z. Zhi, Y. Liu, B. Li, X. Zhang, Y. Lu, D. Shen, X. Fan, Effects of thermal annealing on ZnO films grown by plasma enhanced chemical vapour deposition from $Zn(C_2H_5)2$ and CO_2 gas mixtures, J. Phys. D. Appl. Phys. 36 (2003) 719–722.

[54] M. Cui, X. Wu, L. Zhuge, Y. Meng, Effects of annealing temperature on the structure and photoluminescence properties of ZnO films, Vacuum 81 (2007) 899–903.

[55] S. Tneh, Z. Hassan, K. Saw, F. Yam, H. Hassan, The structural and optical characterizations of ZnO synthesized using the ''bottom-up'' growth method, Physica B 405 (2010) 2045–2048.

[56] D. Muthee, B. Dejene, Effect of annealing temperature on structural, optical, and photocatalytic properties of titanium dioxide nanoparticles, Heliyon 7(6) (2021) e07269.

[57] J. Tauc, R. Grigorovici, A. Vancu, Optical properties and electronic structure of amorphous germanium, Phys. Status Solidi B. 15 (1966) 627–637.

[58] G. Fang, D. Li, B.Yao, Influence of post-deposition annealing on the properties of transparent conductive nanocrystalline ZAO thin films prepared by RF magnetron sputtering with highly conductive ceramic target, Thin Solid Films 418 (2002) 156–162.

[59] D. Speaks, Effect of concentration, aging, and annealing on sol gel ZnO and Al-doped ZnO thin films, Int. J. Mech. Mater. Eng. 15 (2020) 1-14.

[60] S. Rajendran, M. Khan, F. Gracia, J. Qin, V. Gupta, S. Arumainathan, Ce^{3+}-ion-induced visible-light photocatalytic degradation and electrochemical activity of ZnO/CeO_2 nanocomposite, Sci. Rep. 6 (2016) 1–11.

[61] K. Salim, W. Azzaoui, A. Kacha, Effect of Mn Doped and Mn+Sn Co-doping on the properties of ZnO thin films, Int. J. Thin Film Sci. Technol. 10 (2021) 233–237.

https://doi.org/10.30799/jacs.260.24100302

Cite this Article as: Hakim Q.N.M. Al-arique, Sameerah S.S. Alqadasy, Nabeel M.S. Kaawash, S.Q. Chishty, K.A. Bogle, Synthesis of Ag-doped lanthanum nanoparticles using simple wet chemical process in alkaline medium; and characterization of optical, morphological and structural properties, J. Adv. Chem. Sci. 10(3) (2024) 803–807.